HHS Public Access

Author manuscript

Nano Lett. Author manuscript; available in PMC 2017 September 24.

Published in final edited form as:

Nano Lett. 2016 December 14; 16(12): 7357–7363. doi:10.1021/acs.nanolett.6b02577.

The effect of cage shape on nanoparticle-based drug carriers: Anti-cancer drug release and efficacy *via* receptor blockade using dextran-coated iron oxide nanocages

Sham Rampersaud[a], **Justin Fang**[a,b], **Zengyan Wei**[a,b], **Kristina Fabijanic**[a], **Stefan Silver**[c], **Trisha Jaikaran**[c], **Yuleisy Ruiz**[c], **Murielle Houssou**[c], **Zhiwei Yin**[a,b], **Shengping Zheng**[a,b], **Ayako Hashimoto**[f,g], **Ayuko Hoshino**[f], **David Lyden**[f], **Shahana Mahajan**[c,d,*], and **Hiroshi Matsui**[a,b,e,*]

[a]Department of Chemistry, Hunter College, City University of New York, 695 Park Avenue, New York, NY 10065 (USA)

[b]Department of Chemistry, The Graduate Center of City University of New York, 365 Fifth Avenue, New York, NY 10016 (USA)

[c]Department of Medical Laboratory Sciences, Hunter College, City University of New York, 425 East, 25th Street, New York, NY 10010 (USA)

[d]Brain Mind Research Institute, Weill Cornell Medical College, 413 East 69th Street, New York, NY 10021 (USA)

[e]Department of Biochemistry, Weill Cornell Medical College, 413 East 69th Street, New York, NY 10021 (USA)

[f]Children's Cancer and Blood Foundation Laboratories, Departments of Pediatrics, and Cell and Developmental Biology, Drukier Institute for Children's Health, Meyer Cancer Center, Weill Cornell Medicine, New York, New York 10021 (USA)

[g]Department of Obstetrics and Gynecology, Faculty of Medicine, University of Tokyo, Tokyo 113-8655 (Japan)

Abstract

Although a range of nanoparticles have been developed as drug delivery systems in cancer therapeutics, this approach faces several important challenges concerning nanocarrier circulation, clearance, and penetration. The impact of reducing nanoparticle size on penetration through leaky blood vessels around tumor microenvironments *via* enhanced permeability and retention (EPR) effect has been extensively examined. Recent research has also investigated the effect of nanoparticle shape on circulation and target binding affinity. However, how nanoparticle shape

*to whom correspondence should be sent. hmatsui@hunter.cuny.edu, smahajan@hunter.cuny.edu.

[a]Department of Chemistry and Biochemistry, Hunter College and Graduate Center of the City University of New York, New York, NY 10065

[b]Department of Biochemistry, Weill Medical College of Cornell University, 413 E. 69th Street, New York, NY 10021

Author Contributions

The manuscript was written through contributions of all authors.

Supporting Information. Proliferation assay and immunohistochemistry of human lung fibroblast (WI-38) and controls, Experimentals for cell culture and the assays. These materials are available free of charge via the Internet at http://pubs.acs.org."

affects drug release and therapeutic efficacy has not been previously explored. Here, we compared the drug release and efficacy of iron oxide nanoparticles possessing either a cage shape (IO-NCage) or a solid spherical shape (IO-NSP). Riluzole cytotoxicity against metastatic cancer cells was enhanced three-fold with IO-NCage. The shape of nanoparticles (or nanocages) affected the drug release point and cellular internalization, which in turn influenced drug efficacy. Our study provides evidence that the shape of iron oxide nanoparticles has a significant impact on drug release and efficacy.

Graphical abstract

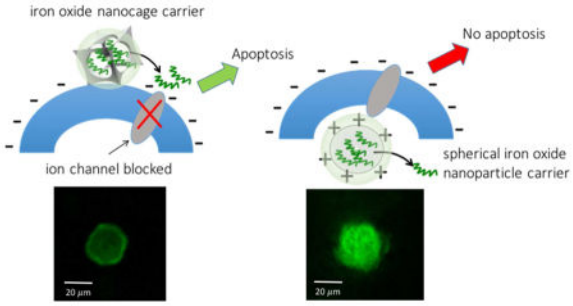

Keywords

Nanoparticles; Drug Delivery; Cancer; Nanoparticle Shape; Nanocage

A wide spectrum of nanoparticle-based drug carriers have been developed to release large doses of drugs in targeted locations, such as tumor sites, assuming nanoparticles can target them actively or passively.[1, 2] Drugs can reach tumor sites as molecules diffuse through complex biobarriers created by an abnormal extracellular matrix (ECM) in the tumor microenvironment; however, nanoparticles typically remain at the near-vascularized regions of tumors.[3, 4] While the characteristic feature of tumor microenvironment EPR allows nanoparticles to reach the vessel walls at the edge of tumor sites, they are still absent in the avascular region of the microenvironment due to an insufficient diffusion rate of larger nanoparticles (as compared to drug molecules) through the complex ECM.[5] The strong affinity of nanoparticles to the ECM also prevents their penetration into the avascular area of the tumor.[6, 7] From studies addressing the issue of deficient nanocarrier diffusion, researchers have observed that nanoparticles less than 50 nm in diameter improve biodistribution, clearance, and escape from phagocytosis as compared to larger nanoparticles,[2, 8–13] Yet, the penetration of nanoparticles through biobarriers is not still efficient enough to translate into clinical applications.[12, 14–16] Given this limitation, mechanisms for drug release at the tumor vasculature or at the ECM around the tumor need to be developed to reduce the distance the drug has to diffuse from the nanoparticles to the tumor tissue.[5, 16] Despite the requirement of such a sophisticated release strategy, it is desirable to keep the nanocarrier structure as simple as possible for scale-up of nanocarrier production.[16]

While the effect of nanoparticle size for drug delivery has been the focus of clinical nanotechnology studies, nanoparticle shape also has been explored. Studies have mostly examined solid nanoparticles and nanorods and found that nanoparticle shape significantly influences fluid dynamics, cellular uptake, and mechanical and binding properties in transvascular transport.[12, 17–20] The impact of nanoparticle shape on drug release and resulting efficacy, however, has not been previously explored. As stated above, the point of drug release before endocytosis is important if high diffusion of drug molecules is required for targeting the tumor microenvironment through perivascular ECMs.

The surface area of nanoparticles is a key component to how nanoparticle shape affects drug-loading capacity and release. For a given nanoparticle size, a cage structure has a much larger surface area than a solid structure. Therefore, we compared the drug release and resulting efficacy from nanoparticles with and without an open-cavity (Fig. 1a). Inorganic nanocages have been developed that contain a single pore and are less than 15 nm in diameter which is within the size range pertinent to medical interests, particularly penetration of biobarriers, such as the blood-brain barrier (BBB).[21] Most of these nanocages have been examined with respect to catalytic and optical properties related to medical imaging and thermo-therapeutics.[22–29] Previously, mesoporous iron oxide nanoparticles 200 nm in diameter were developed by etching pores for gene delivery application.[30] Here, we specifically compared iron oxide nanocages (IO-NCages) and iron oxide solid spherical nanoparticles (IO-NSPs). Inorganic nanocages less than 15 nm in size can be fabricated by controlling crystalline face-dependent ion adsorption/desorption rates on seed nanocrystals.[29] Through the ion exchange *via* this strategy, iron oxide nanocages can be generated in high yield and monodispersity.[31] The iron oxide nanoparticle is one of the most pursued carriers and contrast agents in the theranostic field due to its low toxicity and characteristic size/shape-dependent magnetic property.[9, 32, 33] Iron oxide nanoparticles have been approved to treat iron-deficiency anaemia and applied to reduce the early staging of lymph node metastases among prostate and testicular cancer patients.[21]

In our study, riluzole as a glutamate release inhibitor was incorporated into the IO-NCage cavity and attached onto the IO surface. Drug-incorporated IO-NCages and IO-NSPs in the size range of 15 ± 2.5 nm were subsequently capped by catechol-functionalized dextran for the comparison of drug release and efficacy (Fig. 1a). Iron oxide nanoparticles capped by dextran, a neutral and hydrophilic polymer (Fig. 1b), have been approved by the US Food and Drug Administration as MRI contrast agents.[34] The porous nature of dextran,[35] allows drugs to be released at a controlled rate. Riluzole was delivered to metastatic osteosarcoma cells *via* release from IO-NCages and IO-NSPs. This agent limits glutamate secretion from cells by blocking sodium ion channels,[36] thereby preventing activation of glutamate receptors that utilize glutamate as a signaling molecule.[37] Based on this blocking mechanism, metabotropic glutamate receptor-expressing tumor cells[38] (e.g., those from breast cancer, melanoma, prostrate cancer and osteosarcoma) that secrete and utilize glutamate for enhancing their growth can be treated by riluzole (Fig. 1a).[37, 39–41] Riluzole delivery to osteosarcoma cells by IO-NCages was two times higher compared to neat riluzole. Surprisingly, riluzole delivery by IO-NSPs was less effective than even neat riluzole treatment. The difference in drug delivery by nanoparticle shape depended in part on the point of drug release. Zeta potential analysis indicated that the IO-NCage screens the charge

of drug molecules by incorporating them in the cavity, important for the fate of localization around ion channels. Our data show that nanocarrier shape indeed influences the extent of efficiency of drug delivery.

To study the effect of nanoparticle shape on drug cytotoxicity, we first synthesized IO-NCages in the size range of 15 ± 2.5 nm by etching cubic nanocrystal seeds *via* galvanic exchange reactions (Fig. 2).[31] IO-NCages were then compared with commercially available IO-NSPs. TEM micrographs in Fig. 2a and 2b show the cage shape and hollow cavity of iron oxide nanocages and the electron diffraction pattern in Fig. 3c indicates the single crystalline nature of these nanoparticles. Riluzole was incorporated in the IO-NCages by incubating for 1 hour in DMSO and drug incorporation was confirmed by quantifying *via* HPLC. With the protocol used in this study, each IO-NCage and IO-NSP contains 30 molecules of riluzole, quantified by the amount of riluzole molecules remaining in the supernatant. After the drug was encapsulated into the IO-NCages, the cavities were protected by a catechol-functionalized dextran capping agent (Fig. 1b). We chose to conjugate dihydrocaffeic acid (DHCA) with dextran for the stable capping of the IO-NCage cavity because the catechol group of DHCA has one of the highest affinities toward iron oxide.[9, 42, 43] Dextran is porous, hydrophilic, and neutral polymer used to cap various commercially available nanoparticles for medical applications,[44] This characteristic structure was expected to balance drug release and retention inside the nanocage cavity *via* controlling the thickness of coating.

Analysis of DAPI-staining showed that survival LM7 metastatic osteosarcoma cells in riluzole released from IO-NCages was 18%, almost two times lower than the survival of free riluzole-treated LM7 cells (39%; Fig. 3a, blue bars). To evaluate the effect of nanoparticle shape on drug efficacy, spherical IO-NSPs with no cavity, similar in size to the IO-NCages, were capped by DHCA-dextran after non-covalent attachment of riluzole molecules. IO-NSPs containing 30 molecules of riluzole per nanoparticle were incubated with LM7 cells. Total number of surviving cells (DAPI-stained) in riluzole released from IO-NSPs was three times higher and even two times higher than that observed with IO-NCages and neat drug molecules, respectively (Fig. 3a, blue bars). The number of proliferating cells (Fig. 3a, green bars), positive for the Ki-67 assay, was consistently decreased compared to the trend found in DAPI-stained cells (*i.e.,* proliferating LM7 cells in riluzole released from IO-NCages was 18%, almost two times lower than the proliferation of free riluzole-treated LM7 cells as 41%). The increased efficacy of riluzole treatment with IO-NCages was further confirmed by probing the number of TUNEL-positive apoptotic cells (Fig. 3a, red bars). In Fig. 3b, percentage of apoptotic cells was calculated by dividing the number of apoptotic cells by the number of DAPI-positive cells for each delivery method. Strikingly, 88% of the DAPI-positive cells were TUNEL-positive in the samples treated with the riluzole-loaded IO-NCages. In contrast, free riluzole-treated samples showed only 20% TUNEL positivity and only 13% of DAPI-positive cells were TUNEL positive for riluzole-loaded IO-NSPs.

These results show that riluzole released from IO-NCages was more cytotoxic against LM7 cells compared to riluzole released from IO-NSPs or free riluzole. Neat IO-NCages and IO-NSPs had little effect on total cell number and apoptosis. According to our findings, riluzole efficacy in LM7 osteosarcoma cell apoptosis cells can be enhanced when the drug is

released from IO-NCages, as compared to IO-NSPs, indicating that the shape and the structure of nanocarriers influence in drug delivery and resulting efficacy.

Riluzole molecules induce more apoptosis to cancer cells by blocking ion channels, preventing glutamate receptor activation on the plasma membrane.[45] Supporting this apoptotic mechanism, our control study demonstrated that human lung fibroblasts (WI-38) were associated with reduced drug efficacy *via* IO-NCage delivery due to the diminished expression of glutamate receptors (Fig. S1). Proliferation of WI-38 cells (Fig. S1) was almost three times higher than that of LM7 cells (Fig. 3a) in the same riluzole-IO-NCage incubation (70% versus 24% respectively). The observation that WI-38 cells express glutamate receptors three times less than LM7 cells (Fig. S2) supports the hypothesis that the riluzole nanocage delivery is markedly less effective in WI-38 cells, as compared to LM7 cells.

This apoptotic mechanism of receptor blockade suggests that riluzole efficacy depends on the point of drug release around cells. We hypothesized that the superior cytotoxic effect of riluzole with IO-NCages, as compared to the IO-NSPs, was due to the high payload and release of riluzole at the membrane of LM7 cells. To validate this hypothesis, we labeled IO-NCages and IO-NSPs by FITC dyes and probed the location of nanoparticles around LM7 cells after one hour of incubation. When dye-conjugated catechols were co-adsorbed with dextran-catechols in the consistent concentration on IO-NCages and IO-NSPs, respectively, confocal micrographs showed that IO-NCages localized on the membrane (Fig. 4a and b, upper panel) while IO-NSPs were incorporated into the LM7 cells (Fig. 4a and b, lower panel). Insets are confocal images of stained membranes depicting the corresponding focused plane in the z-direction. To quantify the difference of nanoparticle populations inside the LM7 cell, integrated fluorescence intensities in the center of nanoparticles in Fig. 4b were normalized by integrated fluorescence intensity at the cell's edge. After this normalization, fluorescence intensity of IO-NSPs was found to be 3.4 times higher than that observed for IO-NCages, supporting faster internalization of IO-NSPs in LM7 cells. This observation indicates that IO-NCages adhere to the membrane without cell penetration for a longer time, allowing the drug to be released directly to ion channels, while the IO-NSPs are quickly internalized into the cells, resulting in less effective receptor blockade (Fig. 4c).

Nanoparticle surface charge is a major factor regulating nanoparticle internalization. Recently, positively charged silica nanoparticles were reported to internalize into cells faster than negatively charged nanoparticles.[46] In our work, the charge (as probed by zeta potential measurements) of riluzole-incorporated IO-NCages was more negative (0.08 ± 0.01) than that of IO-NSPs (1.5 ± 0.20 mV). These findings indicate that more positively-charged IO-NSPs are quickly internalized, rendering the drug ineffective in blocking membrane ion channels (Fig. 4c). The data also suggest that IO-NCages have ability to screen charges of drugs *via* incorporation in the cavity, which could be advantageous to deliver highly charged drugs into targeted areas.

In conclusion, when riluzole was incorporated inside cage-shaped IO-NCages, this anti-cancer drug was released onto LM7 cell membranes, inducing apoptosis by blocking ion channels and glutamate receptors. The cytotoxic effect of riluzole was two times higher with

IO-NCage carriers than with neat drug incubation and drug delivery with spherical shaped solid IO-NSPs was three times less efficient than IO-NCages. Thus, the shape of nanocarriers indeed matters in drug deliver and cytotoxicity. One reason for increased efficiency in drug delivery with IO-NCages is the charge-screening effect on the nanoparticle surface. When drugs are conjugated with nanoparticle carriers, the charge of drugs could affect the overall charges of hybrids. However, IO-NCages effectively screen the charge of drugs by incorporation inside the cavity and stable capping with the DHCA-dextran. In the case of riluzole efficacy against metastatic osteosarcoma cells, charge is important in that nanocarriers need to release the drug at the outer membrane before endocytosis to effectively block membrane ion channels and prevent glutamate release in order to induce apoptosis. Our study showed that the faster endocytosis observed with IO-NSPs resulted in less effective blockade of ion channels displayed on outer cells and in turn less effective apoptosis of osteosarcoma cells. It should be noted that the majority of tumors express glutamate receptors, although these receptors are very heterogeneous due to different subunit combinations.[47] Since selective ligands for targeting particular glutamate receptor subunits are available,[48] IO-NCages conjugating these targeting agents and glutamate release inhibitors, such as riluzole, could be useful in targeted therapy applications for specific cancer types.

Cage-shaped nanoparticles with a cavity could be applied as universal drug carriers for newly designed drugs, enabling either penetrating membranes or adhering to cell surfaces, regardless of the drug charge. As discussed in the Introduction, drug nanocarriers could be more effective with certain types of tumors (*e.g.*, unvascularized metastatic sites where nanoparticles cannot penetrate due to the lack of EPR) if the drug can be released before nanocarriers are internalized *via* endocytosis and then penetrate through the complex tumor microenvironment from the entrance of tumor sites with the shortest travel distance.[21] Recently, many human tumors were found to express P-selectin, an inflammatory cell adhesion molecule, on tumor cells and in tumor vasculature, whereas normal tissues exhibit little expression.[49] Drug-encapsulated P-selectin-targeted nanoparticles could arrest tumor sites at the endothelium, and the enhanced drug efficacy was observed through the efficient drug diffusion through ECMs to multiple metastatic sites, assisted by ionizing radiation.[49] IO-NCages could be effective for a similar drug delivery scheme whereby P-selectin or related membrane molecules are targeted by IO-NCages and then the anti-cancer agent is released in high concentration from the IO-NCages at the endothelium, dependent on the diffusion of drugs to tumor sites through ECMs. In our system, drug release could also be assisted by magnetic IO-NCage-based hyperthermia at targeted locations if the nanocages further penetrate tumor tissues. This approach could represent an alternative way to deliver drugs deep into the tumor microenvironment without relying on the EPR-based targeting. Inorganic nanocages can be fabricated by a simple protocol and thus complex synthesis pathways are not necessary, enabling scaled up production without excessive separation processes. The size of the nanocage cavity allows incorporation of drugs and RNAs in high payloads, reducing the amount of material required and treatment cost. Notably, riluzole incorporated into liposomes with a diameter of 88 nm, compared to neat riluzole molecules, was shown to yield better efficacy and less accumulation in the liver *in vivo*.[50] Due to their

cage shape, smaller size and neutral charge, IO-NCages may allow for enhanced drug efficacy *in vivo.* The enormous potential of nanocages needs to be tested in future research.

Methods

Materials

Manganese (II) acetate, oleylamine, oleic acid, iron (II) perchlorate, and 2-(N-morpholino) ethanesulfonic acid (MES) were purchased from Sigma-Aldritch. *p*-Xylene, dimethyl sulfoxide (DMSO), dihydrocaffeic acid (DHCA), and fluorescein isothiocyanate (FITC) were purchased from Acros Organics. 1-ethyl-3-[3-dimethylaminopropyl]carbodiimide (EDC) and N-hydroxysuccinimide (NHS) were purchased from Thermo Scientific. Dextran, amino, 40000 MW was purchased from Molecular Probes. Dihydrocaffeic acid was purchased from Alfa Aesar.

Iron oxide nanocage (IO-NCage) synthesis

Iron oxide nanocages were synthesized by a modified version of a previously published method.[31] 0.17 g of manganese (II) acetate, 0.82 mL of oleylamine, and 0.16 mL of oleic acid were added to 15 mL of p-xylene in a three-necked 50 mL flask with a reflux condenser. The flask was heated to 90° C in air under magnetic stirring, then 1 mL of deionized water was rapidly injected into the flask. The reaction mixture was heated at 90° C for 1.5 hours, producing Mn_3O_4 nanoparticles. 1 mL of 2.0 M aqueous iron(II) perchlorate solution was added and the mixture maintained at 90° C for an additional 1.5 hours to produce the iron oxide nanocages by galvanic replacement. After cooling, the solution was centrifuged and the supernatant removed, mixed with 15 ml ethanol, and centrifuged to collect the nanocages, which were then dispersed in hexane.

FITC conjugation with DHCA-dextran

First, 100 mg (2.5 μmol) aminodextran (molecular weight 40 KDa, 10 amines per molecule), 4.6 mg (25 μmol) DHCA, 4.8 mg (25 μmol) 1-ethyl-3-[3-dimethylaminopropyl]carbodiimide (EDC), and 2.9 mg (25 μmol) N-hydroxysuccinimide (NHS) were dissolved in 1 mL dimethyl sulfoxide and 1 mL pH 6 buffer containing 0.1M 2-(N-morpholino)ethanesulfonic acid (MES) and 0.5M NaCl and reacted overnight. The catechol-dextran was condensed with ethanol and collected by centrifugation. The pellet was dissolved in 1 mL H_2O with sonication, then frozen and lyophilized. To fluorescently label the product dextran with FITC, 30 mg of the DHCA-dextran was dissolved in 0.3 mL of pH 8.3 0.1M phosphate buffer, and 3 mg of FITC dissolved in 0.1 mL DMSO was added. The solution was reacted overnight, and then the product was condensed with ethanol and collected by centrifugation. The pellet was dissolved in 0.3 mL H_2O with sonication, purified using a Zeba spin desalting column, 7K MWCO (Thermo Scientific), frozen and lyophilized.

IO-NCage/IO-NSP drug loading, capping by DHCA-dextran, and labeling by FITC

To load riluzole on IO-NCages, riluzole hydrochloride (25 mg) is dissolved in DMSO- (1 mL, 99.9%) prior to incubation with Iron Oxide to yield a 92.4 mM stock solution. The IO-NCage (0.02 mL, 25 mg/mL) suspension in DMSO (99.9%) was loaded with riluzole

(0.065mL, 92.4 mM) solution. The solution was incubated and placed on a rocker with vigorous shaking for 1 hour. The drug in the IO-NCage solution was mixed with DMSO and DHCA-dextran (0.035 mL, 50 mg/mL). In the resulting solution (50 mM), the DHCA-dextran capped the cavity of IO-NCage and sealed its drug content. The solution is left on a rocker for an hour. The hybrid, drug-IO-NCage mixture, was centrifuged at 13,300 RPM for 10 minutes and then washed with the same volume of DHCA-dextran (0.1 mL, 50 mg/mL) for re-suspension after light vortexing and sonication (20 seconds). A control IO-NCage sample with no drugs should be prepared using the same concentration of iron content (25 mg/mL) and the same ration of DHCA-dextran (50 mg/mL) used in the drug-nanocage hybrid sample. For the IO-NSPs, first the suspension was washed by the chloroform *via* centrifugation at 13,300 RPM. After the solvent was exchange with DMSO (1 mL, 99.9%) three times, riluzole was loaded on IO-NSP's. Riluzole hydrochloride (25 mg) was dissolved in DMSO- (1 mL, 99.9%) prior to incubation with IO-NSPs to yield a 92.4 mM stock solution. The IO-NSP suspension in DMSO (99.9%) (0.02 mL, 25 mg/mL) was loaded with riluzole (0.065mL, 92.4 mM) solution, and then the solution was incubated and placed on a rocker with vigourous shaking for 24 hours. Then, the solution of drug-loaded IO-NSPs was mixed with a solution of DMSO and DHCA-dextran (0.035 mL, 50 mg/mL) to be consistent with the capping condition of the IO-NCage. A control IO-NSP sample with no drug was prepared using the same concentration of iron content (25 mg/mL) and the same ration of DHCA-dextran (50 mg/mL) used in the drug-nanocage hybrid sample. To label IO-NCages and IO-NSPs with the FITC dye, after an IO-NCage suspension in DMSO (99.9%) (0.02 mL, 25 mg/mL) was added to the FITC-DHCA-dextran conjugate (0.004 mL, 6.5 mg/mL), the sample was diluted by DMSO (.5 mL, 99.9 %) and then left on a rocker for 3 hours. After centrifuging down the sample for 10 minutes at 13,300 RPM, the sample was washed five times with a 1 mL volume of DMSO. After washing, 100 μL of DMSO (99.9%) was added and re-suspended *via* sonication. Next, 5 μL of this suspension was added to the seeded cell samples and incubated for 3 hours. The seeded cells were gently washed with Millipore water and followed the fixing protocol with 4% PFA. A Z-stack of these cells were imaged by Nikon A1 Confocal Microscope on different cross sections of these cells. The integrated fluorescence intensity of middle slice of cells was normalized by the one for the edge to quantify the nanoparticle content in each cell for the comparison of localization around the cell.

Cell Culture

LM7 cells were maintained in DMEM supplemented with 4.5% glucose, 1mM pyruvate, 10% fetal bovine serum, 100 units/mL penicillin and 100 μg/mL streptomycin. Cells were passaged every 4 days. Cells were maintained at 37°C with 95% air and 5% CO_2. For experiments when indicated, cells were seeded in DMEM media without glutamate, penicillin and streptomycin and 0.5% fetal bovine serum.

Drug delivery to cells in vitro

First, 1.5×10^4 cells were seeded onto polylysine coated coverslips in 24 well plates. Twenty-four hour later the LM7 cells were treated with riluzole (100 μM). The drug-contained IO-NCages or IO-NSPs (.002 mL) was placed within the seeded LM7 cell suspension and gently mixed with pipetting for even dispersion within the sample. The LM7

cells were fixed 48 hour post-treatment. Three different control samples are added to sequential wells. A DMSO control (.001 mL, 99.9%), neat riluzole hydrochloride control (.001 mL, 50 mM), and neat IO-NCage/IO-NSP controls (.002 mL, 30 mg/mL) were added to the 1 mL LM7 cell seeded suspensions in the wells. All samples were tested in triplicates, and allowed these samples to incubate in a 37° incubator for 48 hours.

Proliferation assay

Post drug treatment, the cells were fixed in 4% paraformaldehyde for 10 min and permeabilized in 0.2 % triton X-100 for 5 min. The cells were washed well with 1X Phosphate buffered saline (PBS) and then blocked with 10% bovine serum albumin made in 1X PBS. Immunocytochemistry was carried out using primary antibodies such as anti-rabbit Ki-67 followed by ALEXA 488-conjugated anti-rabbit secondary antibody. The samples were mounted in mounting media (Molecular Probes) containing DAPI for nuclear staining. Images were captured at 20X magnification using a Zeiss fluorescence microscope. The images were used for counting DAPI positive and Ki-67 positive cells. At least five images were used from each sample and the experiments were repeated at least four times.

TUNEL assay

TUNEL assay was performed using the *in situ* cell death detection kit from Roche as per manufacturer's instructions. Briefly, after cells were fixed with 4% paraformaldehyde and permeabilized in 0.2% Triton X-100, the TUNEL assay was carried by incubating the fixed cells with the TUNEL reagent containing TMR red labeled nucleotides at 37° C for 1 hour. The samples were washed in 1X PBS and mounted in mounting media containing DAPI. Fluorescent images were captured using a Zeiss fluorescence microscope at 20X magnification. The total number of DAPI positive cells and total number of TUNEL positive cells were counted from at least five images from each sample. Each experiment was repeated four times.

Supplementary Material

Refer to Web version on PubMed Central for supplementary material.

Acknowledgments

Funding Sources

The National Institute on Minority Health and Health Disparities (NIMHD) of the National Institutes of Health (NIH).

This work was supported by the National Institute on Minority Health and Health Disparities (NIMHD) of NIH (MD007599) for nanoparticle fabrications and imaging, and H.M. also acknowledges NIH/NCATS (UL1TR00457) for analytical assays. D.L. acknowledges the Children's Cancer and Blood Foundation, the Paduano Cancer Research Fund, the Champalimaud Foundation, and the Weill Cornell Medicine Daedalus Fund and Clinical and Translational Science Center Awards, and A.H. acknowledges the Susan Komen For The Cure Fellowship for cell cultures and a part of *in vitro* assays and immunohistochemistry. S.R. acknowledges Patrick Kelly for the quantification of drug by HPLC. We thank Dr. Eugenie Kleinerman from M D Anderson Cancer Center for the gift of LM7 cells.

ABBREVIATIONS

ECM	extracellular matrix
IO-NCage	iron oxide nanocage
IO-NSP	iron oxide nanosphere
EPR	enhanced permeability and retention
BBB	blood-brain barrier
DHCA	dihydrocaffeic acid

References

1. Lusic DD. Nature. 1996; 380:561–2. [PubMed: 8606781]
2. Caldorera-Moore M, Guimard N, Shi L, Roy K. Expert Opin Drug Deliv. 2010; 7:479–495. [PubMed: 20331355]
3. Dreher MR, Liu W, Michelich CR, Dewhirst MW, Yuan F, Chilkoti A. J Natl Cancer Inst. 2006; 98:335–44. [PubMed: 16507830]
4. Yuan F. Semin Radiat Oncol. 1998; 8:164–75. [PubMed: 9634493]
5. Peiris PM, Bauer L, Toy R, Tran E, Pansky J, Doolittle E, Schmidt E, Hayden E, Mayer A, Keri RA, Griswold MA, Karathanasis E. ACS Nano. 2012; 6:4157–68. [PubMed: 22486623]
6. Allen TM. Nat Rev Cancer. 2002; 2:750–763. [PubMed: 12360278]
7. Adams GP, Schier R, McCall AM, Simmons HH, Horak EM, Alpaugh RK, Marks JD, Weiner LM. Cancer Res. 2001; 61:4750–4755. [PubMed: 11406547]
8. Sykes EA, Chen J, Zheng G, Chan WC. ACS Nano. 2014; 8:5696–5706. [PubMed: 24821383]
9. Lee N, Yoo D, Ling D, Cho MH, Hyeon T, Cheon J. Chem Rev. 2015; 115:10637–10689. [PubMed: 26250431]
10. Yoo B, Ma K, Zhang L, Burns A, Sequeira S, Mellinghoff I, Brennan C, Wiesner U, Bradbury M. Bioorg Med Chem. 2015; 23:7119–7130. [PubMed: 26462054]
11. Champion JA, Katare YK, Mitragotri S. J Control Release. 2007; 121:3–9. [PubMed: 17544538]
12. Toy R, Peiris PM, Ghaghada KB, Karathanasis E. Nanomedicine. 2014; 9:121–134. [PubMed: 24354814]
13. Choi HS, Liu W, Misra P, Tanaka E, Zimmer JP, Itty Ipe B, Bawendi MG, Frangioni JV. Nat Biotechnol. 2007; 25:1165–1170. [PubMed: 17891134]
14. Xu R, Zhang G, Mai J, Deng X, Segura-Ibarra V, Wu S, Shen J, Liu H, Hu Z, Chen L, Huang Y, Koay E, Huang Y, Liu J, Ensor JE, Blanco E, Liu X, Ferrari M, Shen H. Nat Biotechnol. 2016; 34 Article Preview. doi: 10.1038/nbt.3506
15. Sharma G, Valenta DT, Altman Y, Harvey S, Xie H, Mitragotri S, Smith JW. J Control Release. 2010; 147:408–412. [PubMed: 20691741]
16. Peer D, Karp JM, Hong S, Farokhzad OC, Margalit R, Langer R. Nat Nanotech. 2007; 2:751–760.
17. Truong NP, Whittaker MR, Mak CW, Davis TP. Expert Opin Drug Deliv. 2015; 12:129–142. [PubMed: 25138827]
18. Christian DA, Cai S, Garbuzenko OB, Harada T, Zajac AL, Minko T, Discher DE. Mol Pharm. 2009; 6:1343–1352. [PubMed: 19249859]
19. Alkilany AM, Thompson LB, Boulos SP, Sisco PN, Murphy CJ. Adv Drug Deliv Rev. 2012; 64:190–199. [PubMed: 21397647]
20. Scheinberg DA, Villa CH, Escorcia FE, McDevitt MR. Nat Rev Clin Oncol. 2010; 7:266–276. [PubMed: 20351700]
21. Schroeder A, Heller DA, Winslow MM, Dahlman JE, Pratt GW, Langer R, Jacks T, Anderson DG. Nat Rev Cancer. 2012; 12:39–50.

22. Xia Y, Li W, Cobley CM, Chen J, Xia X, Zhang Q, Yang M, Cho EC, Brown PK. Acc Chem Res. 2011; 44:914–924. [PubMed: 21528889]
23. Macdonald JE, Bar Sadan B, Houben LIP, Banin U. Nat Mater. 2010; 9:810–815. [PubMed: 20852616]
24. Yin Y, Rioux RM, Erdonmez CK, Hughes S, Somorjai GA, Alivisatos AP. Science. 2004; 304:711–714. [PubMed: 15118156]
25. Métraux GS, Cao YC, Jin R, Mirkin CA. Nano Lett. 2003; 3:519–522.
26. González E, Arbiol J, Puntes VF. Science. 2011; 334:1377–1380. [PubMed: 22158813]
27. Peng Z, You H, Wu J, Yang H. Nano Lett. 2010; 10:1492–1496. [PubMed: 20297767]
28. Peng S, Sun S. Angew Chem Intl ed. 2007; 46:4155–4158.
29. Wei Z, Matsui H. Nat Commun. 2014; 5:3870. [PubMed: 24828960]
30. Cao B, Qiu P, Mao CB. Microsc Res Tech. 2013; 76:936–941. [PubMed: 23913581]
31. Oh MH, Yu T, Yu S-H, Lim B, Ko K-T, Willinger M-G, Seo D-H, Kim BH, Cho MG, Park j-H, Kang K, Sung Y-E, Pinna N, Hyeon T. Science. 2013; 340:964–968. [PubMed: 23704569]
32. Shavel A, Benito Rodríguez-González B, Pacifico J, Spasova M, Farle M, Liz-Marzán LM. Chem Mater. 2009; 21:1326–1332.
33. Colombo M, Carregal-Romero S, Casula MF, Gutiérrez L, Morales MP, Böhm IB, Heverhagen JT, Prosperi D, Parak WJ. Chem Soc Rev. 2012; 41:4306–4334. [PubMed: 22481569]
34. Bullivant JP, Zhao S, Willenberg BJ, Kozissnik B, Batich CD, Dobson J. Int J Mol Sci. 2012; 14:17501–17510.
35. Zhang X, Wang JC, Lacki KM, Liapis AI. J Phys Chem B. 2005; 109:21028–21039. [PubMed: 16853725]
36. Martin D, Thompson MA, Nadler JV. Eur J Pharm. 1993; 250:473–476.
37. Willard SS, SK. Int J Biol Sci. 2013; 9:728–742. [PubMed: 23983606]
38. Teh J, Chen S. Wiley Interdiscip Rev Membr Transp Signal. 2012; 1:211–220. [PubMed: 22662310]
39. Speyer CL, Smith JS, Banda M, DeVries JA, Mekani T, Gorski DH. Breast Cancer Res Treat. 2012; 132:565–573. [PubMed: 21681448]
40. Yip D, Le MN, Chan JL, Lee JH, Mehnert JA, Yudd A, Kempf J, Shih WJ, Chen S, Goydos JS. Clin Cancer Res. 2009; 15:3896–3902. [PubMed: 19458050]
41. Akamatsu K, Shibata MA, Ito Y, Sohma Y, Azuma H, Otsuki Y. Anticancer Res. 2009; 29:2195–2204. [PubMed: 19528481]
42. Lee H, Dellartore SM, Miller WM, Messersmith PB. Science. 2007; 318:426–430. [PubMed: 17947576]
43. Amstad ETG, Bilecka I, Textor M, Reimhult E. Nano Lett. 2009; 9:4042–4048. [PubMed: 19835370]
44. Lévesquea SG, Lima RM, Shoicheta MS. Biomaterials. 2005; 26:7436–7446. [PubMed: 16023718]
45. Yu LJ, Wall BA, Wangari-Talbot J, Chen S. Neuropharm. 2016; doi: 10.1016/j.neuropharm.2016.02.011
46. Zhang Y, Yang M, Park JH, Singelyn J, Ma H, Sailor MJ, Ruoslahti E, Ozkan M, Ozkan C. Small. 2009; 5:1990–1996. [PubMed: 19554564]
47. Stepulak A, Rola R, Polberg K, Ikonomidou C. J Neural Transm. 2014; 121:933–944. [PubMed: 24610491]
48. Stepulak A, Luksch H, Gebhardt C, Uckermann O, Marzahn J, Sifringer M, Rzeski W, Staufner C, Brocke KS, Turski L, Ikonomidou C. Histochem Cell Biol. 2009; 132:435–445. [PubMed: 19526364]
49. Shamay Y, Elkabets M, Li H, Shah J, Brook S, Wang F, Adler K, Baut E, Scaltriti M, Jena PV, Gardner EE, Poirier JT, Rudin CM, Baselga J, Haimovitz-Friedman A, Heller DA. Sci Trans Med. 2016; 8:345ra87.
50. Bondì ML, Craparo EF, Giammona G, Drago F. Nanomedicine. 2010; 5:25–32. [PubMed: 20025461]

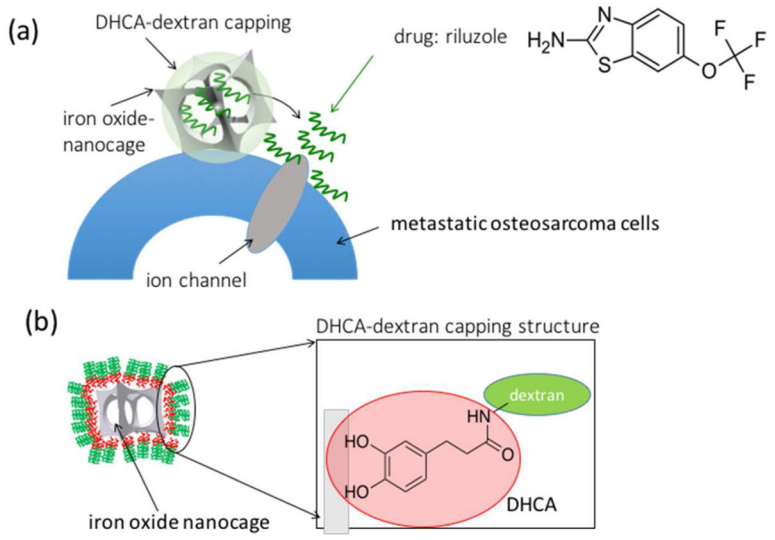

Figure 1.

(a) Schematic to delivery anti-cancer drug of riluzole to metastatic osteosarcoma cells by IO-NCages. Riluzole blocks sodium ion channels to induce apoptosis of cancer cells. The shape of iron oxide nanocarriers affects the localization around the cells, and these locations are important for the efficacy of anti-cancer drugs. (b) Illustration of the DHCA-dextran capping on IO-NCages. The porous, neutral, and hydrophilic dextran is conjugated with DHCA. The catechol group of DHCA enables stable capping on iron oxide nanoparticles.

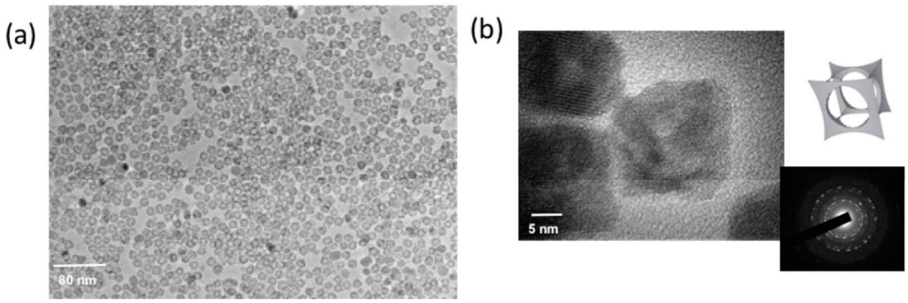

Figure 2.

(a) TEM image of iron oxide nanocages (IO-NCages) in (a) low magnification (b) high magnification. (upper inset) an illustration of IO-NCage (lower inset) An electron diffraction of IO-NCages indicates the single crystalline nature of iron oxide (the facets are assigned as (220), (311), and (400) from the inner circle).

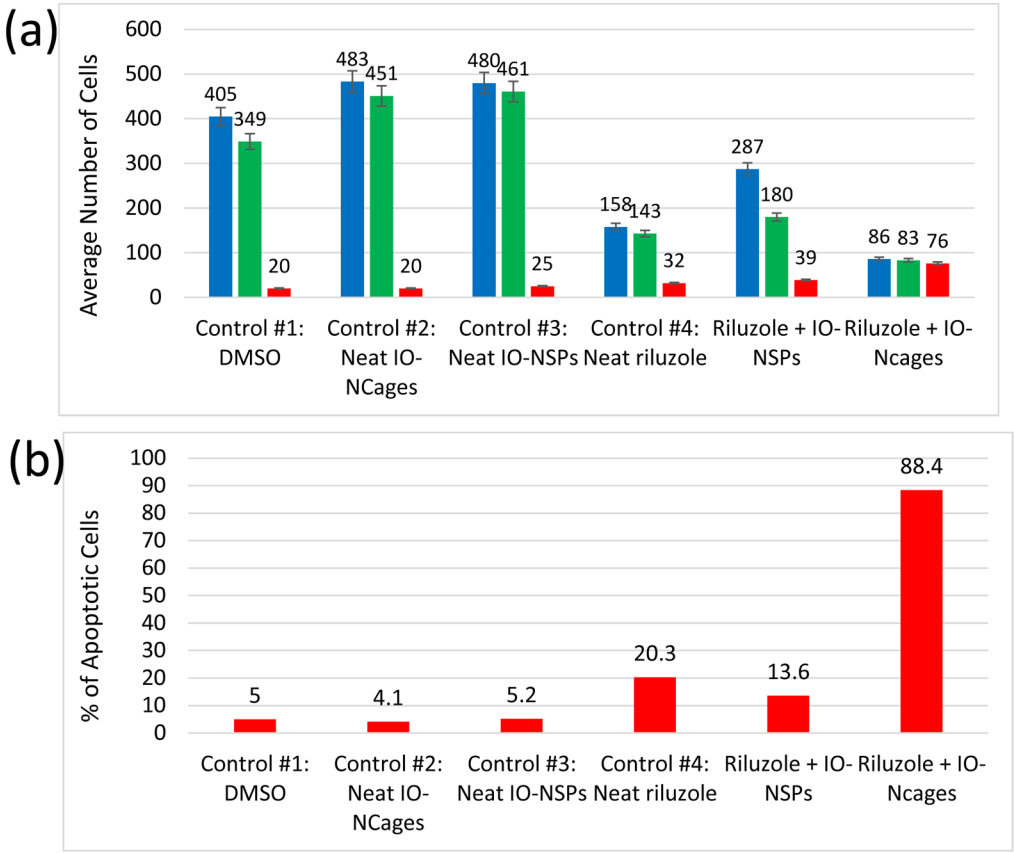

Figure 3.

(a) Total cell viability tested after 48 hr incubation with osteosarcoma cells (LM7) containing drug loaded IO-NCages and IO-NSPs. Blue bars show DAPI staining for total cell numbers, green bars show Ki-67 assay for proliferation, and red bars show TUNEL assay for apoptosis. Controls are neat solvent of DMSO (control #1), neat IO-NCages (control #2), neat IO-NSPs (control #3), and neat riluzole (control #4). Riluzole delivery from IO-NCages reduces the cell viability from 483 cells to 86 cells (18%) as compared to the one by neat riluzole of 39% (405 cells to 158 cells). (b) The percentages of apoptotic cells, calculated by dividing the number of apoptotic cells by the number of DAPI positive cells. Among total LM7 cells, 88% of cells are apoptosis positive after the drug is delivered by IO-NCages, which is much higher than the riluzole delivery by IO-NSPs.

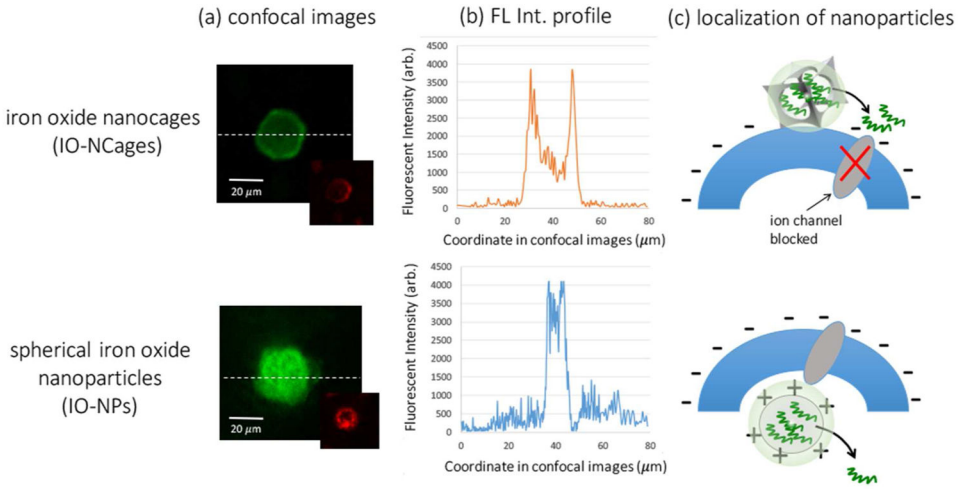

Figure 4.

(a) Confocal images of osteosarcoma cells incubated with iron oxide nanocages (IO-NCages) (upper) and iron oxide spherical nanoparticles (IO-NSPs) (bottom). Green color shows the locations of nanoparticles on the sliced plane of the center of cells in the confocal imaging. Insets in red color show stained membrane for comparison. IO-NCages are localized on the membrane while IO-NSPs are internalized inside the cell after 48 hours of incubation. (b) Fluorescence profile of dotted lines in (a). (c) Illustrations for localizations of IO-NCages (upper) and IO-NSPs (bottom). Based on zeta potential measurements, positively-charged IO-NSPs are quickly internalized in cells while neutral IO-NCages remains longer on membranes so that more riluzole can be released near the location of ion channels which blocks the channel and limit glutamate binding to the receptors.